

# Numerical simulation of tested reinforced concrete beams strengthened by thin fibre-reinforced cementitious matrix jackets

K. Georgiadi-Stefanidi, E. Mistakidis\*, P. Perdikaris and T. Papatheocharis

*Department of Civil Engineering, University of Thessaly, 38334 Volos, Greece*

*(Received March 14, 2010, Accepted August 31, 2010)*

**Abstract.** The paper presents a study on the numerical simulation of the behaviour of conventional reinforced concrete (RC) beams strengthened by thin fibre-reinforced cementitious matrix (FRCM) jackets. The study covers the cases of retrofitting RC beams with or without stirrups with jackets reinforced with longitudinal and transverse steel reinforcement or with light wire mesh. The strengthened RC beams to be modelled were tested under static monotonic and fully reversing cyclic loading. The numerical results show that the numerical model used predicted quite well the experimental results.

**Keywords:** fibre reinforced cementitious composites; seismic strengthening; numerical simulation.

---

## 1. Introduction

A great number of existing reinforced concrete structures are relatively old and were not built according to the current seismic design regulations. Therefore, it is possible that they lack sufficient longitudinal or transverse reinforcement and they don't meet the standards of modern codes. Moreover, especially in the case of old buildings, the structural materials may be of low quality or may exhibit degradation in their mechanical properties due to environmental factors or aging. Therefore, these structures may present weaknesses in ductility, strength and stiffness. Strengthening or retrofitting of this type of structural members can provide a solution against the aforementioned deficiencies and can be proved essential for avoiding damages and loss of life from earthquakes.

Some techniques used for strengthening or repairing of structural concrete members involve the construction of reinforced concrete (RC) jackets (see e.g. Rodriguez and Park 1994, Vadoros and Dritsos 2006), or the attachment of steel plates to the faces of the members (see e.g. Adhikary and Mutsuyoshi 2006). More recently, fibre-reinforced polymers (FRPs) were developed and are used in the form of fabrics, such as carbon fibre-reinforced polymer sheets, wrapped around the structural member (Khalifa and Nanni 2002, Li *et al.* 2009, Doran *et al.* 2009), or in the form of textile reinforced mortar (TRM) jackets (Triantafillou and Papanicolaou 2006). Another method of strengthening or repairing of structural concrete members is the use of ferrocement laminates attached onto the surface of the members (Paramasivam *et al.* 1998).

---

\* Corresponding author, Associate Professor, E-mail: [emistaki@uth.gr](mailto:emistaki@uth.gr)

During the past few decades, the use of fibre-reinforced concrete or cement composites (FRCCs) for the improvement of the performance of structural members has been investigated by many researchers. The addition of steel fibres to conventionally reinforced concrete beams can improve the member's strength and stiffness, while the fibres restrict the growth of cracks (Bentur and Mindess 1983). The parameters that affect the behaviour of FRCCs have been investigated by many researchers (see e.g. Balaguru *et al.* 1992, Banthia and Trottier 1995, Ashour and Wafa 1993, Chunxiang and Patnaikuni 1999, Daniel and Loukili 2002). More recently, significant progress has been achieved in the development of high-performance fibre-reinforced cementitious composites. These composites use fine aggregates or fine sand that improve the overall characteristics of the cement mixtures, as it was demonstrated by various researchers. They are able to provide crack growth control, significantly higher tensile strength and high ductility and energy absorption capacity (Naaman and Reinhardt 1996). Lately, cementitious composites were introduced, which are based on a micromechanically engineered cementitious matrix reinforced with tailored polymer fibres, giving even more superior tensile and bending response (Li 2003).

Different types of jackets for strengthening and rehabilitation of RC members can be fabricated based on high-performance fibre-reinforced cementitious composites. Among the huge number of contributions in this field, we mention here the cases of jackets from slurry infiltrated mat concrete (SIMCON) (Oluokun and Haghayeghi 1998, Krstulovic-Opara and Al-Shannag 1999, Dogan and Krstulovic-Opara 2003) slurry infiltrated fibre concrete (SIFCON) (Naaman *et al.* 1993) and high-strength fibre-reinforced concrete with different types of fibres (Shannag and Alhassan 2005, Haddad *et al.* 2007). All the aforementioned types of high-performance fibre-reinforced cementitious composites have the advantage that can be applied to form the jacket using relatively small thickness.

The aim of this paper is the efficient numerical simulation of the bending behaviour of conventional RC structural members strengthened by relatively thin cast-in-place jackets. It must be noted that, as no axial load is applied, the present study deals with the simulation of beam behaviour exclusively. For the jackets a high-strength cementitious matrix was used, in which hooked-end steel fibres were added with a volumetric content of 0.8%. The main application of the FRCM jackets under study in this work is the seismic strengthening of existing RC buildings. The proposed jackets have also the advantage of having relatively small thickness. Thus, they can provide considerable strength and ductility to the existing members without the addition of significant mass.

In this paper, four different types of strengthened RC beam members were investigated. Their differences lie on the presence or the absence of transverse reinforcement in the core member that was strengthened and also, on the type of the reinforcement of the jacket. The beam specimens were tested under static monotonic and fully reversing cyclic four-point bending (equal positive and negative displacements producing positive and negative bending moments respectively) up to failure. For comparison reasons and in order to determine the increase in tensile strength and energy absorption capacity that the FRCM jackets could provide, conventional RC beam specimens, identical to the strengthened members in terms of geometric and material properties, were tested under similar loading conditions.

In order to obtain the required experience and verify the precision of the proposed simulation methods, a quite simple numerical model had to be initially employed. For this reason, it was decided to first simulate the behaviour of a conventionally RC beam member under static monotonic loading. A realistic three-dimensional finite element model was first created, followed by a simpler two-dimensional one. The validity of this simpler model was established by comparing its

results with those obtained by the three-dimensional model and the corresponding experimental ones. The two-dimensional numerical simulation of the four types of the strengthened beam specimens, subjected to static monotonic and fully reversing cyclic loading followed. For the analysis, the MSC-MARC finite element software code was used. Both the numerical and the experimental results lead to similar conclusions concerning the behaviour of the strengthened beams which depend mainly on the type of steel reinforcement that is present in the strengthened member and in the jacket.

## 2. Types of strengthened beam specimens

### 2.1 Geometry and configurations

The geometric characteristics of the strengthened beam specimens are shown in Fig. 1. The reinforced concrete member which is strengthened with the FRCM jacket is made of conventional concrete. The cross-sectional dimensions of the conventional RC beam members are  $150 \times 200$  mm (see Fig. 2), which, after applying a 35 mm-thick FRCM jacket, become  $220 \times 270$  mm for the strengthened member. The beam specimens are simply supported with a span of 1600 mm.

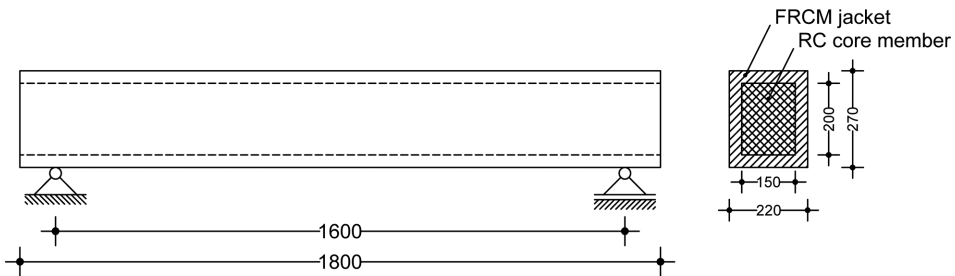


Fig. 1 Geometric characteristics of the RC beam specimen strengthened by an FRCM jacket (dimensions in mm)

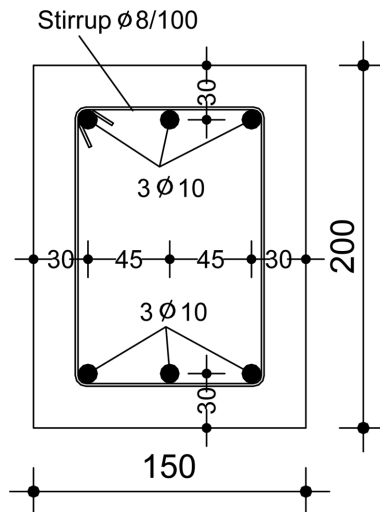


Fig. 2 Cross-section dimensions of the conventional RC beam specimens (dimensions in mm)

For the strengthened RC member two different cases were considered; beams with longitudinal steel reinforcement and closely spaced stirrups and beams with longitudinal reinforcement and no transverse reinforcement. It should be noted here that the decision to consider the strengthened beam member without shear reinforcement, is due to the fact that existing older RC structures usually have very low transverse steel reinforcement ratios. It is characteristic that in the case of RC structures that have collapsed due to various earthquakes in Greece during the last years, structural members were found to be very poorly reinforced with stirrups placed at 40 or even 50 cm. Therefore, it was decided to include in this study RC beams without transverse steel reinforcement, in order to verify the effectiveness of the jacketing scheme in similar cases which are very common in practice. Furthermore, the main application of the examined FRCM jackets, as already mentioned, is the seismic strengthening of existing buildings. For the strengthening FRCM jackets, two different cases were also considered for comparison reasons, that is, thin FRCM jackets with longitudinal and transverse steel reinforcement and jackets reinforced with a light steel wire mesh (T131). Therefore, four types of beam specimens were produced, mentioned as J1, J2, J3 and J4. The longitudinal steel reinforcement of the inner member consists of three top and bottom steel

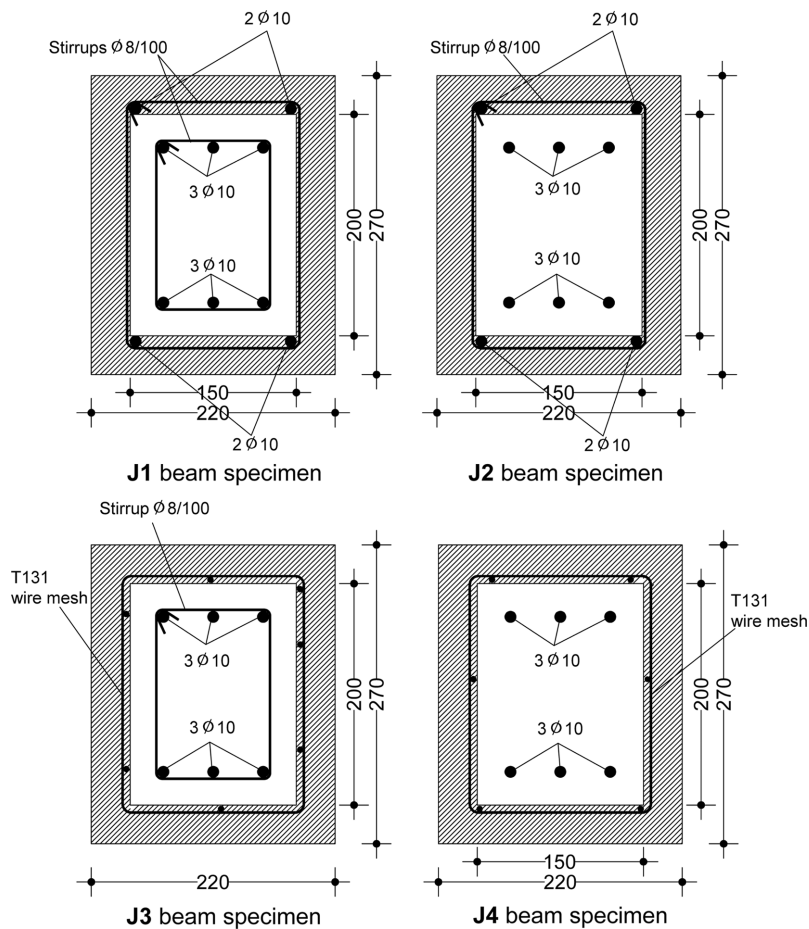


Fig. 3 Cross-section of the four types of FRCM strengthened beam specimens (dimensions in mm). Types of reinforcement are given in Table 1.

Table 1. Types of reinforcement used for each one of the considered strengthened beam types

	J1	J2	J3	J4
Core reinforcement	Longitudinal and transverse	Longitudinal but no transverse	Longitudinal and transverse	Longitudinal but no transverse
Jacket reinforcement	Longitudinal and transverse	Longitudinal and transverse	Wire mesh	Wire mesh

rebars with a diameter of 10 mm (3Ø10). For J1 and J3 beam specimens, the transverse steel reinforcement consists of stirrups with a diameter of 8 mm placed at a spacing of 100 mm (Ø8/100), while J2 and J4 specimens have no transverse reinforcement. Regarding the FRCM jackets, for the first two cases (J1 and J2), the longitudinal steel reinforcement consists of two top and bottom steel rebars with a diameter of 10 mm (2Ø10). The transverse steel reinforcement consists of stirrups with a diameter of 8 mm placed at a spacing of 100 mm (Ø8/100). In the last two cases (J3 and J4) the jackets are reinforced with a steel mesh which consists of longitudinal and transverse wires with a diameter of 5 mm and spacing of 150 mm (T131). Fig. 3 presents the cross-sectional dimensions of the four types considered, while Table 1 summarizes the differences in the reinforcement types.

For comparison reasons, simply supported conventional RC beam members with geometric and material properties and reinforcement similar to that of the strengthened beams were also studied under static monotonic and fully reversing cyclic bending.

## 2.2 Materials

### 2.2.1 Fibre reinforced cementitious matrix

For the FRCM jackets, a high-strength cementitious matrix with hooked-end steel fibres was used. The mix design of the FRC matrix is given in Table 2. The volumetric content of fibers in the mix was  $v_f = 0.8\%$ . The steel fibres had a circular cross-section, diameter  $d_f = 0.4$  mm and an aspect ratio (length/diameter) equal to 70 (see Fig. 4). According to the specifications of the manufacturer,

Table 2. Mix design of the FRC matrix

Cement	682 kg/m <sup>3</sup>
Solid additive (custom reactive components)	13.9 kg/m <sup>3</sup>
Fine sand	1421 kg/m <sup>3</sup>
Hooked fibres	61 kg/m <sup>3</sup>
Water	231 kg/m <sup>3</sup>
Superplasticizer	9.1 kg/m <sup>3</sup>

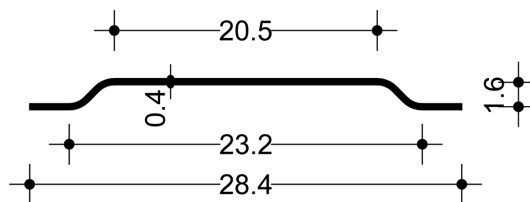


Fig. 4 Dimensions of the steel fibres used (in mm)

the yielding stress of the steel fibres was equal to 1400 MPa. The cementitious matrix material had an average splitting tensile strength of 8 MPa (150 mm diameter  $\times$  300 mm long cylinders) and a compressive cube strength of 80 MPa (150  $\times$  150  $\times$  150 mm cubes).

### 2.2.2 Concrete

The concrete used for the conventional RC beams had an average splitting tensile strength of 2.6 MPa and a compressive cube compressive strength of 30 MPa.

### 2.2.3 Steel reinforcement

The steel rebars for the longitudinal and transverse reinforcement had a yielding strength of 550 MPa and the T131 steel wire mesh a yielding strength of 500 MPa.

## 3. Experimental testing

Six (6) conventional reinforced concrete beams (see Fig. 2) were tested under static monotonic and fully reversing cyclic load. Eight (8) similar beams were strengthened with cast-in-place 35-mm thick high-strength FRCM jackets, according to the four different strengthening types presented in Section 2. This resulted in two specimens for each strengthening type. One beam of each strengthening type was tested under monotonic loading while the other one under fully reversing cyclic loading. All static cyclic tests were performed under displacement-control (midspan deflection) for two full cycles at specified displacement values (Papatheocharis and Perdikaris 2009). The load was applied at two points, symmetrically positioned along the beam, creating four point bending conditions. The constant moment region had a span of 380 mm.

To measure the midspan deflection of the beams, two direct current differential transformers (DCDTs) were used, one on each side of the beam, attached on independent simply supported aluminium hollow bars, monitoring the relative displacement between the top fiber of the midspan cross-section and the two end support cross-sections at mid-height (see Fig. 5). In addition to the beam's midspan deflection, the stroke of the hydraulic jack and the applied load were also recorded. The fully reversing cyclic loading was applied through an appropriate system of top and bottom



Fig. 5 Instrumentation of the FRCM strengthened beams

steel plates and tension threaded rods, which allowed the application of downward and upward loading at 2 points. At the two “hinge” and “roller” end supports, the specimens were tied down to the floor beam reaction frame through tension threaded rods to accommodate for reaction to the upwardly applied load at load reversals (see Fig. 6).

For the sake of brevity but in order to grasp quickly the differences in the responses of the various types of tested specimens, only selected experimental results will be presented in this section while the rest will be presented together with the corresponding numerical ones. The diagrams of the applied maximum bending moment vs. midspan deflection for the RC and strengthened beam specimens subjected to monotonic flexural loading are presented in Fig. 7. The presence of the fibre-reinforced jacket results in an increase of the stiffness and considerable increase of the carrying capacity of the conventional RC beams, especially in the case of the jackets with conventional reinforcement (J1, J2).

For a better comparison of the flexural response under fully reversing cyclic loading, the envelope M vs.  $\delta$  diagrams of the conventional RC beams and those strengthened with the FRCM jacket are



Fig. 6 Experimental set-up for the FRCM strengthened beam under fully reversing cyclic loading

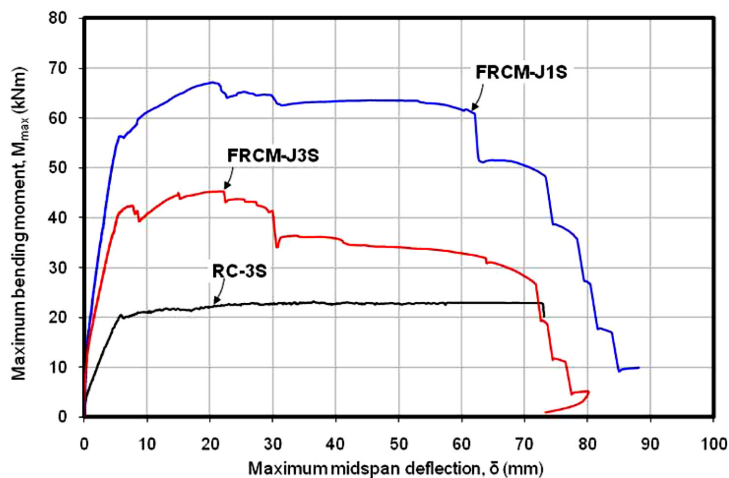


Fig. 7 Flexural response of various specimens subjected to static monotonic bending: (RC-3S: RC beam, FRCM-J1S: J1 type jacket, FRCM -J3S: J3 type jacket)

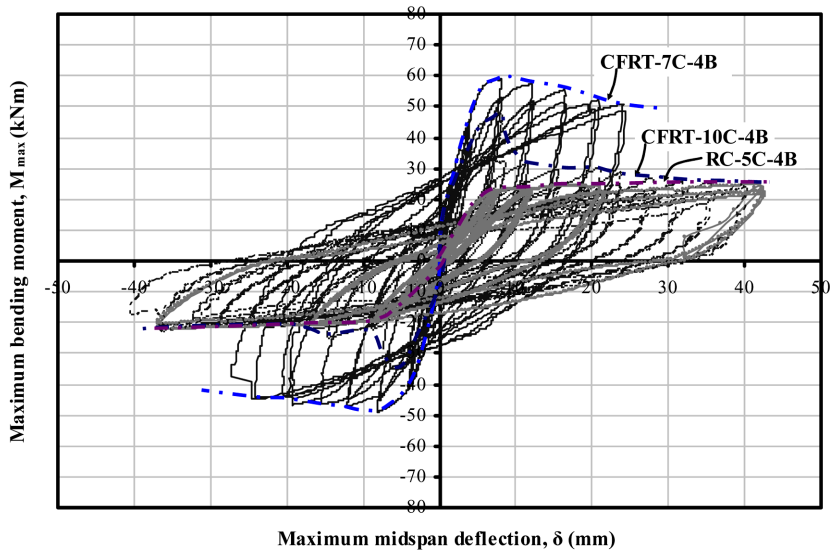


Fig. 8 Overall flexural response (envelope) of standard RC and strengthened beams subjected to static fully reversing cyclic bending (FRCM-J1C: J1 type jacket, FRCM-J3C: J3 type jacket, RC-5C: RC beam)

presented in Fig. 8. The following preliminary conclusions can be drawn for the flexural response of the strengthened beams under fully reversing cyclic loading:

- (a) the hysteresis response of the strengthened beams with longitudinal and transverse steel reinforcement is far superior to that of those with steel wire mesh. The maximum carrying capacity at a midspan deflection of  $\pm 8$  mm is diminished after cycling down to that of the conventional RC beams only when the applied midspan deflection reaches a value of at least  $\pm 32$  mm (5 times that causing first yielding in the longitudinal rebars of the jacket), with a more abrupt decrease in the case of the strengthened beams with steel wire mesh.
- (b) right after the yielding of the longitudinal reinforcement in the jacket, the strengthened beams exhibited a rather considerable energy absorption capacity of up to 2 times that of the RC beams in the case of the jackets with longitudinal rebars. With further cycling of the strengthened beams, the energy absorption ability at an applied midspan deflection of  $\pm 24$  mm showed an almost 5- and 2-fold increase for the case of the jackets with longitudinal rebars and steel wire mesh, respectively. For applied midspan deflections above  $\pm 12$  mm, the absorbed energy for the strengthened beams with longitudinal rebars is about  $2 \div 2.5$  times that of the strengthened beams with steel wire mesh.

#### 4. Numerical simulation

The numerical simulation of the considered beam experiments is a difficult task, due to the complexity of the system and the various nonlinear phenomena that appear, which should be taken properly into account, such as:

- cracking in the concrete and in the cementitious matrix;
- plastification of steel reinforcement elements;
- nonlinear bond response between the cementitious matrix and the steel fibres.

Moreover, several simulation problems appeared while trying to formulate the numerical models, which had to be solved efficiently. At first, a three-dimensional (3D) modelling resulted in huge computational times especially in the case of cyclic loading (of the order of 5-6 CPU hours on a SUN X4450 computer). For this reason, effective two-dimensional (2D) models are proposed in this paper. A comparison of the results based on the 2D and 3D models for the conventional RC beam member will be given in the next section, in which it is verified that a 2D model may be very effective in problems like the one treated here.

#### 4.1 Geometric and material properties

The models utilized 2D finite elements which proved effective for the simulation of bending behavior and were able to provide realistic results, just like the 3D finite elements, as it will be shown later in Section 5. It should be noted that the effectiveness of the 2D numerical simulation schemes results from the more or less two-dimensional deformation patterns that develop in all tested specimens. However, the 2D simulation is not able to account for the actual stress and strain fields that develop as a result of the confinement provided by the transverse reinforcement. Nevertheless, these effects seem not to affect the global response of the beams.

Each model consists of various finite element meshes, its components, which overlap, actually connected in the same nodes. Two types of finite elements are used, plane-stress and truss elements. The plane-stress elements are used for the simulation of the conventional concrete, the cementitious matrix and the fibres, while the truss elements are used for the simulation of the reinforcement bars. The various components of the model are explained in the following.

##### 4.1.1 Conventional concrete

The conventional concrete was modelled through plane-stress isoparametric finite elements which were equipped with the stress-strain relationship depicted in Fig. 9(a). The loss of tensile strength after cracking was modelled through a softening branch having a slope equal to  $k_s^C$ . In compression, an elastoplastic behaviour is assumed due to the confinement provided by the transverse reinforcement and/or the FRCM jackets. The elasticity modulus for these elements was taken equal to 32 GPa and the Poisson's ratio  $\nu = 0.16$ . The thickness of these elements was taken equal to the width of the strengthened RC beam's cross-section, i.e. 150 mm.

##### 4.1.2 Fibre reinforced cementitious matrix

In order to better understand the modelling for the FRCM, the behaviour of the material under tension should be briefly presented. When the tensile force is rather low, it is undertaken through the tensile stresses that develop in the cementitious matrix. For higher stresses, the cement matrix cracks and the tensile stresses are transferred to the steel fibres. Initially, however, the steel fibres behave elastically and, as the tensile force increases, the steel fibres start to pull-out from the cementitious matrix under a mixed friction-plastification mechanism (Georgiadi-Stefanidi *et al.* 2010). Finally, the steel fibres are completely pulled-out from the cementitious matrix and no more tensile force can be resisted.

Here, this type of complex behaviour is simplified by means of the decoupling of the contribution of the cementitious matrix from that of the steel fibres. The contribution of the cementitious matrix is taken into account by means of a specific layer of plane-stress isoparametric finite elements which are equipped with a stress-strain relationship that exhibits an elastoplastic behaviour for

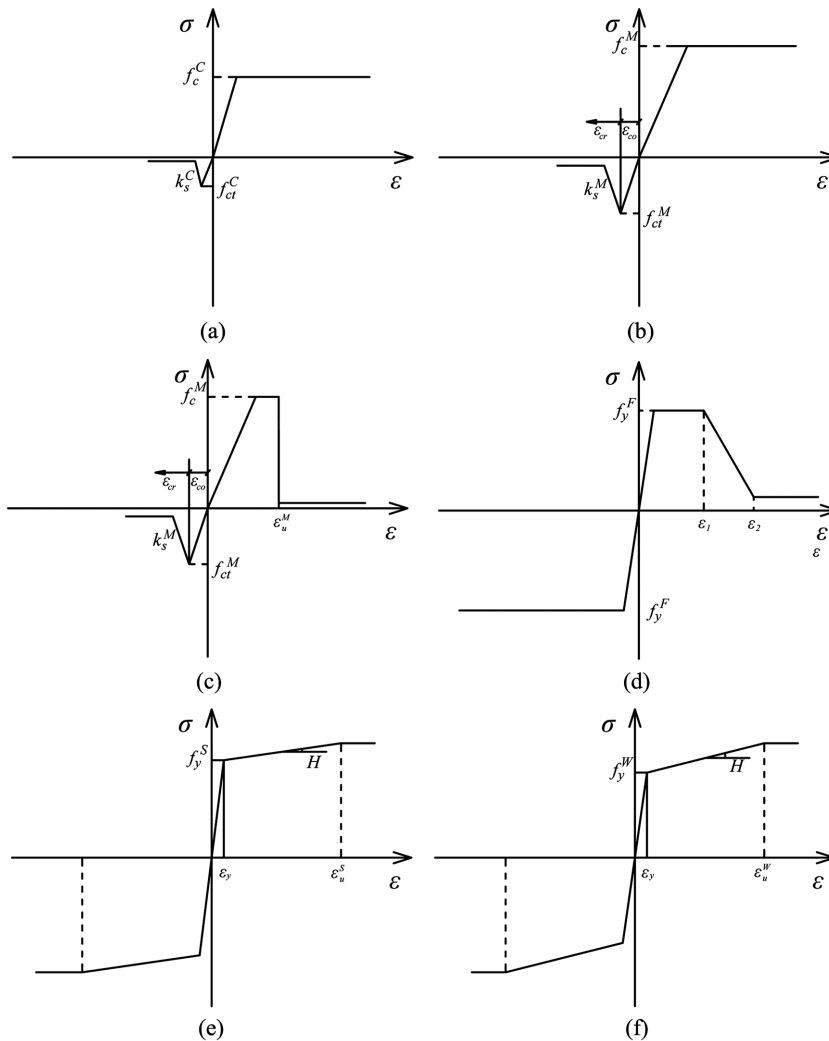


Fig. 9 Stress-strain relationships considered in this work for the (a) conventional concrete, (b) confined cementitious matrix, (c) unconfined cementitious matrix, (d) steel fibres, (e) longitudinal and transverse reinforcement and (f) steel wire mesh. The parameters displayed on the figure are given in Table 3

compressive loading and a cracking behaviour for tensile loading. In order to be as accurate as possible in the material modelling, two different cases are considered for the behaviour of the FRCM in compression, according to the confinement conditions. The regions that lie outside of the centerlines of the transverse reinforcements (see Fig. 10) are considered to be unconfined while the region inside the transverse reinforcement is considered to be confined. The confined regions are equipped with the stress-strain relationship of Fig. 9(b), while the unconfined ones are equipped with the stress-strain relationship shown in Fig. 9(c). In this last case, the compressive strength is almost zeroed for a strain larger than 0.004 (see e.g. Papanikolaou and Kappos 2007). The slope of the softening branch  $k_s^M$  is the same as in the case of the conventional concrete. The modulus of elasticity was taken equal to 35.5 GPa and the Poisson's ratio  $\nu = 0.2$ . Moreover, as they are plane-stress isoparametric elements, their thickness is taken equal to the corresponding thickness of the

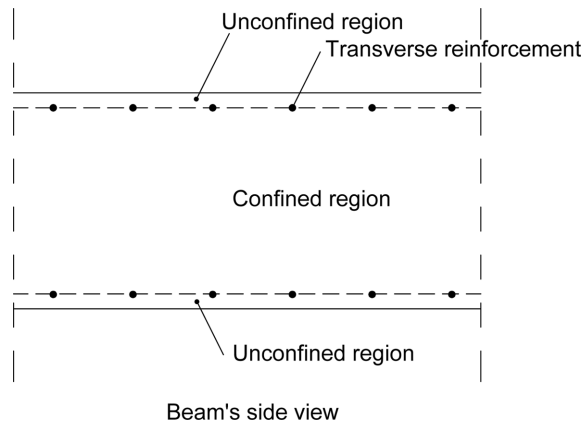


Fig. 10 The considered confined and unconfined regions

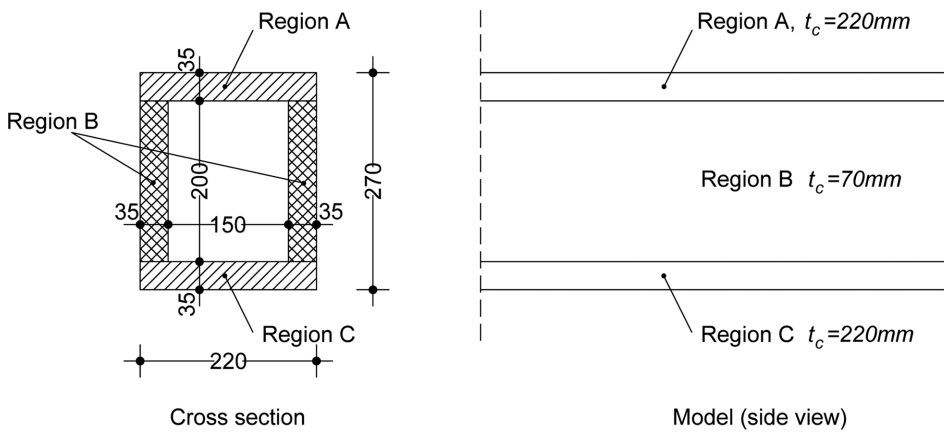


Fig. 11 Assignment of different thickness for the finite elements of the regions representing the FRCM

FRCM jacket region that they model. Three regions can be distinguished, the top and bottom FRCM regions denoted by A and C in Fig. 11, where the thickness of the elements is equal to the width of the member's cross-section (i.e. 220 mm) and the side FRCM region denoted by B, where the thickness assigned to the matrix elements is equal to the sum of the widths of the left and right parts of the jacket (i.e. 70 mm).

The contribution of the pull-out mechanism of the steel fibres is taken into account through another layer of plane-stress isoparametric finite elements which are connected at exactly the same position with the previous layer of elements. In this way, the elements representing the steel fibres and those representing the cementitious matrix have common nodes and thus, common displacements (see Fig. 12). In this new layer of finite elements, the contribution of the fibres is taken into account in a homogenized way, through an equivalent thickness,  $t_f$  which is obtained by the following relation,

$$t_f = t_c \times a_f \times v_f \tag{1}$$

where  $v_f = 0.8\%$  is the volumetric content of fibres in the cement mixture,  $t_c$  is the thickness of the corresponding region of the cementitious matrix and  $a_f = 0.50$  is a factor which takes into account

the orientation of the fibres in the matrix (see Padmarajaiah and Ramaswamy 2002). Therefore, for the regions of the fibres' F.E. mesh corresponding to regions A and C of the matrix (resp. region B), relation (1) gives  $t_f = 0.88$  mm (resp.  $t_f = 0.28$  mm). The modulus of elasticity for these elements was taken equal to 210 GPa, and the Poisson's ratio  $\nu = 0.3$ .

The stress-strain relationship considered for the fibre-matrix response is shown in Fig. 9(d). The characteristic strains  $\varepsilon_1$  and  $\varepsilon_2$  resulted from an analysis of pull-out experimental results for a single fibre in the cementitious matrix (Georgiadi-Stefanidi *et al.* 2010). The softening branch between the strain values  $\varepsilon_1$  and  $\varepsilon_2$  represents the gradual pull-out of the steel fibre from the cementitious matrix.

#### 4.1.3 Steel reinforcement bars

The finite elements representing the longitudinal and transverse steel reinforcement bars and the steel mesh are two-node, constant cross-section truss elements, connected in the same grid of nodes on which the plane-stress elements are connected. The cross-sectional area of these elements was taken equal to the total area of the corresponding longitudinal and transverse reinforcing bars. That is, for the line of elements representing the top and bottom steel reinforcement of the core RC beam specimen, the cross-sectional area is  $3 \times 78.5 = 235.5$  mm<sup>2</sup> (3Ø10). For the lines of elements representing the stirrups of the core member, the cross-sectional area is  $2 \times 50 = 100$  mm<sup>2</sup> to account for the two vertical legs of the Ø8 stirrup. The longitudinal rebars were assumed to behave elastoplastically with hardening and a modulus of elasticity of 210 GPa. The stress-strain diagram for the rebars and the steel wire mesh are given in Figs. 9(e) and 9(f), respectively. It should be noted that the rebars and the wire mesh had different yield strength.

All the material properties and characteristic stress and strain values for the materials used in this paper are given in Table 3 and depicted in Fig. 9. The one-dimensional laws of this figure are combined with an appropriate yielding criterion (Von Mises for the different kinds of steel and Tresca for the cementitious matrix and for the concrete), in order to take into account the other stress directions. For the different kinds of steel used here, kinematic hardening was used to model the material behaviour after yielding (i.e. considering appropriately the Bauschinger effect).

For the modelling of cracking, the smeared crack approach was employed (deBorst *et al.* 2004), i.e. the cracks are taken into account in an average sense by appropriately modifying the material properties at the integration points of the corresponding finite elements. This approach involves no remeshing and is convenient when the crack orientations are not "a priori" known. The method has been extensively applied and proved to work satisfactorily when the cracks to be modelled are themselves smeared out, as e.g. in reinforced concrete applications. Without going into more details, the method incrementally decomposes the strains (see definitions in Fig. 9) into concrete strains,  $\varepsilon_{co}$  and cracking strains,  $\varepsilon_{cr}$ , i.e.

$$\varepsilon = \varepsilon_{co} + \varepsilon_{cr} \quad (2)$$

therefore allowing the separate treatment of each of them.

However, cracking posed a serious obstacle in the numerical analysis, especially when the cyclic loading was applied. Under the reversing cyclic loading, regions with 2D elements tended to detach from the finite element mesh because of the excessive cracking strains, causing numerical instability and convergence failure of the Newton–Raphson iterative numerical procedure. In order to handle this phenomenon, "stabilizing" elastic low-stiffness elements with an axial stiffness equal to  $E_D \times A_D = 0.1$  kN were added in the finite element mesh. Notice that, due to their very low axial

Table 3. Material properties and characteristic stress and strain values for the materials considered (see Fig. 9)

Confined reinforced concrete
$f_c^C = 30$ MPa $f_{ct}^C = 2.6$ MPa $k_s^C = 10^5$ MPa
Confined cementitious matrix
$f_c^M = 80$ MPa $f_{ct}^M = 8$ MPa $k_s^M = 10^5$ MPa
Unconfined cementitious matrix
$f_c^M = 80$ MPa $f_{ct}^M = 8$ MPa $k_s^M = 10^5$ MPa $\varepsilon_u^M = 0.004$
Fibre-matrix response
$f_y^M = 1000$ MPa $\varepsilon_1 = 0.04$ $\varepsilon_2 = 0.06$
Longitudinal and transverse reinforcement
$f_y^S = 550$ MPa Hardening slope $H = 0.55$ GPa $\varepsilon_u^S = 0.2$
Structural mesh
$f_y^W = 500$ MPa Hardening slope $H = 0.50$ GPa $\varepsilon_u^W = 0.2$
Stabilizing elements
axial stiffness $E_D \times A_D = 0.1$ kN

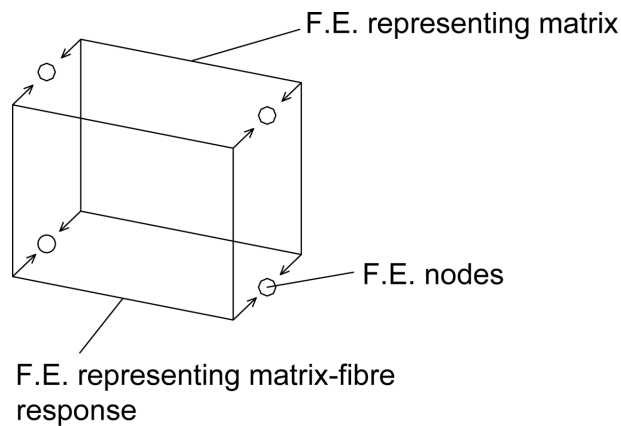


Fig. 12 Coupling of the finite elements representing the cementitious matrix and the steel fibres of the FRCM jacket, at the same nodes

stiffness, the contribution of these elements to the strength of the beam is negligible. Eventually, these stabilizing elements managed to keep-in-place the detaching concrete or matrix elements in the regions where excessive cracking occurred under cyclic loading.

The different sets of finite elements for a typical model (RC beam specimen strengthened by FRCM jacket), as well as the corresponding geometric properties, are shown in Fig. 13. All these sets of elements are actually connected to the same grid of nodes.

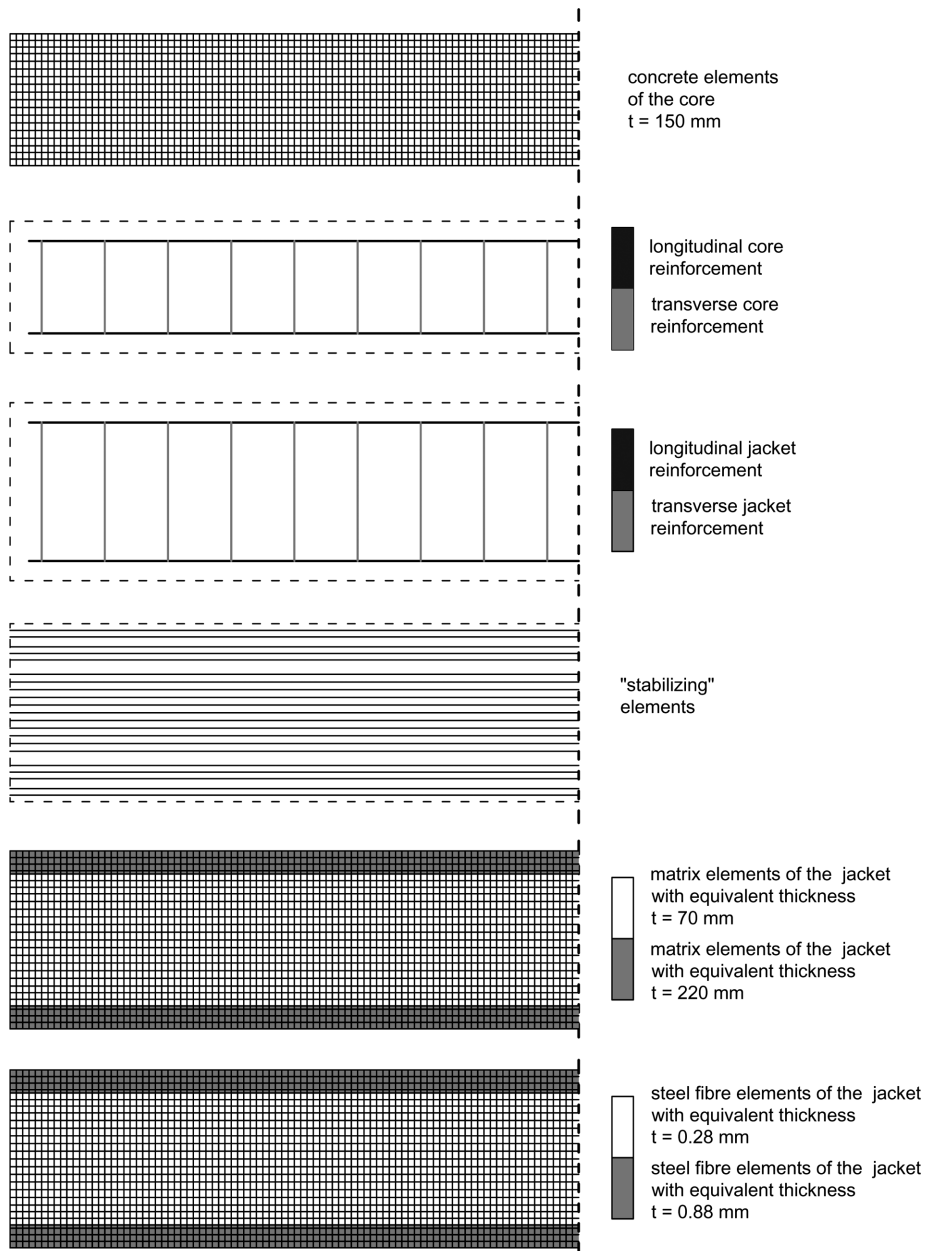


Fig. 13 The different sets of finite elements for the conventional RC beam strengthened with the FRCM jacket

4.2 Boundary conditions – applied load procedure

The simulation of the load application procedure introduced several difficulties, for both the monotonic and cyclic loading, and therefore required a special numerical treatment. In general, it was not possible to apply the load directly to a nodal point of the finite element mesh, because the elastic-plastic and cracking properties of the concrete and/or the matrix caused the elements adjacent to this node to deform significantly, causing a premature failure of the solution algorithm. More specifically, since the applied load caused a compressive stress zone in the neighbouring area of the load application node, stress concentrations and non-realistic stress fields occurred, creating excessive, premature plastification in the concrete. To avoid this phenomenon, a  $220 \times 50 \times 15$  mm steel plate was placed on the upper side of the specimen, through which the load was applied through induced displacements. This adopted loading procedure in the analysis resulted in the normalization of the stress and strain fields in the load application area. On the other hand, during cyclic loading and specifically during load reversal, the applied load produced a tensile stress zone in the applied load region. Even for moderate load values, rather high stress concentration appeared

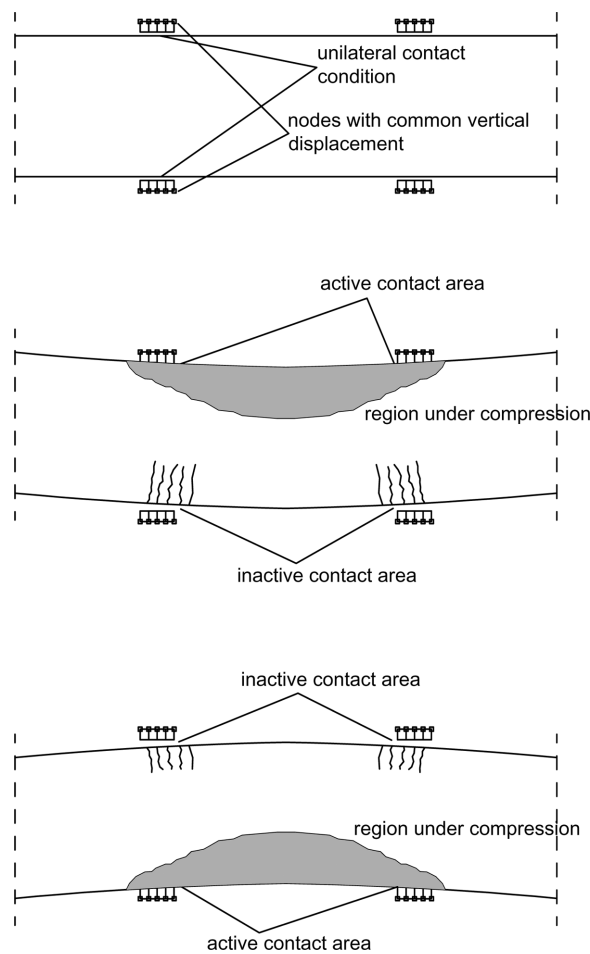


Fig. 14 The two-plate loading system and its function during the cyclic load application

locally, near the node to which the load was applied and thus, non-realistic conditions for cracking were created, destroying the neighbouring elements and leading to premature termination of the numerical process. Therefore, for the application of the cyclic load, a system consisting of two steel plates, one on the top and one on the bottom face of the beam specimen was adopted. Between the plates and the specimen, unilateral contact conditions were assumed. The two plates were connected by kinematical constraints (common vertical displacements) in order to achieve the load application in both directions and so that only compressive forces are imposed on the respective contact surface of the specimen. The assumed detail of the two plate loading system is shown in Fig. 14.

### 4.3 Numerical solution procedure

The solution to the described problem was obtained by using the software code MSC-MARC. A Newton-Raphson iterative procedure was applied to handle the nonlinearities of the problem. The load was applied in the form of an induced displacement  $\delta$  at the top of the specimen at a distance of 190 mm from midspan on each side of the axis of symmetry. The resulting force  $P$  at the points of the incrementally applied displacement was monitored. A relative convergence criterion was adopted based on the residual forces and the relative force tolerance was set to 0.001.

## 5. Behaviour of conventional RC beam

To verify the efficiency of the proposed simulation methods, a 3D and a 2D numerical model of the conventional RC beam specimen under three-point static monotonic bending were initially formulated. For the 3D simulation of the concrete, an eight-node, isoparametric hexahedral element was used (hex8). The longitudinal and transverse rebars were modelled by using 3D straight truss elements with constant cross-section. The elements representing the longitudinal rebars were assigned a cross-sectional area of  $78.5 \text{ mm}^2$ , while those representing the stirrups an area of  $50 \text{ mm}^2$ . The specimen was modelled by 5568 finite elements. The discretization, as well as a detail

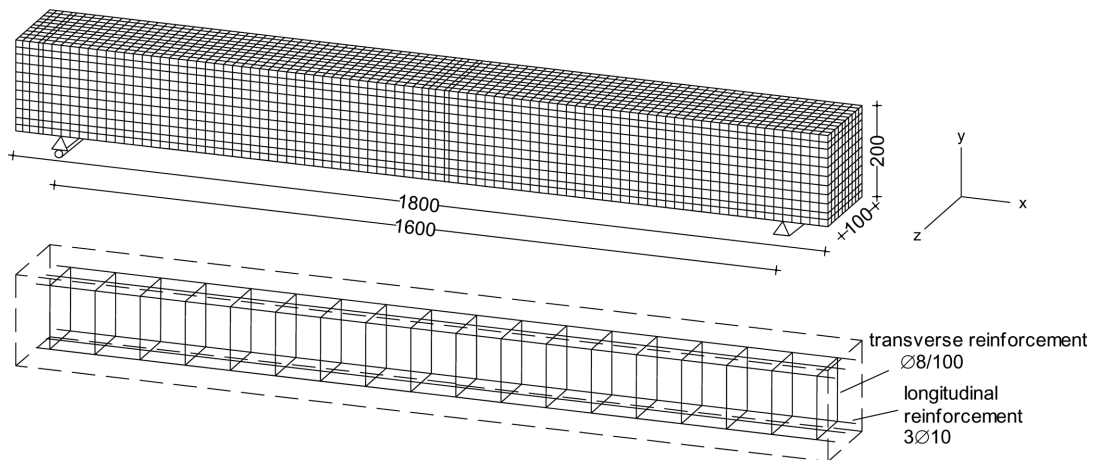


Fig. 15 Details of the finite elements representing concrete and reinforcement for the 3D numerical model (dimensions in mm)

of the elements representing the longitudinal and transverse steel reinforcement are shown in Fig. 15.

The 3D model described above, although accurate, led to a high computational time. Thus, it was decided to employ a simpler 2D model, which would be able to provide reliable results. The rules for the creation of the 2D model are the same as those given in the previous section for the strengthened RC beam members. Here, plane-stress elements for the simulation of the conventional concrete and truss elements for the steel reinforcement were employed. Finally, low stiffness “stabilizing” elements were used in the case of the cyclic loading, similar to the finite elements which represent the steel rebars, in order to avoid the mentioned numerical difficulties. The reinforcing steel elements and the stabilizing elements embedded in the F.E. mesh together with the elements representing the concrete after the discretization are shown in Fig. 16.

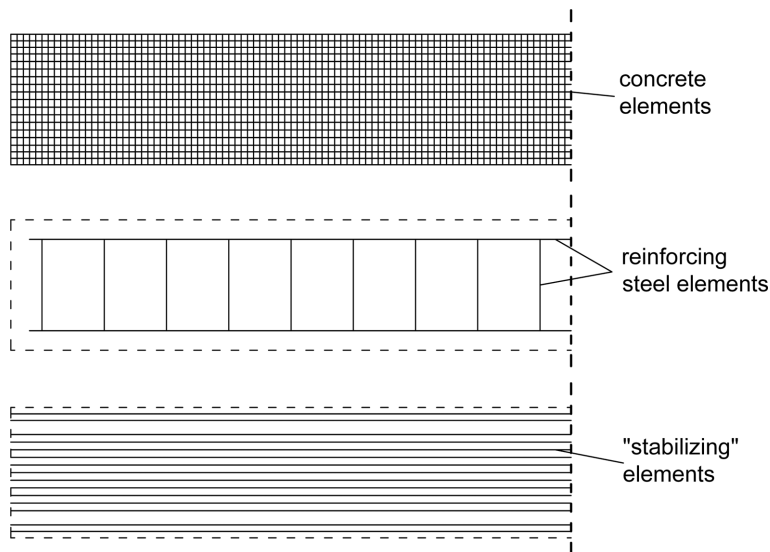


Fig. 16 Details of the finite elements representing concrete, reinforcement and “stabilizing” elements for the 2D numerical model

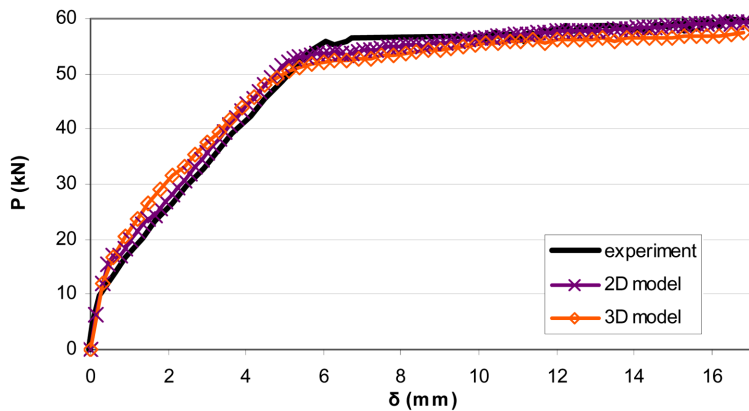


Fig. 17 Comparison of the numerical and experimental results of the original RC beam under static monotonic four-point bending

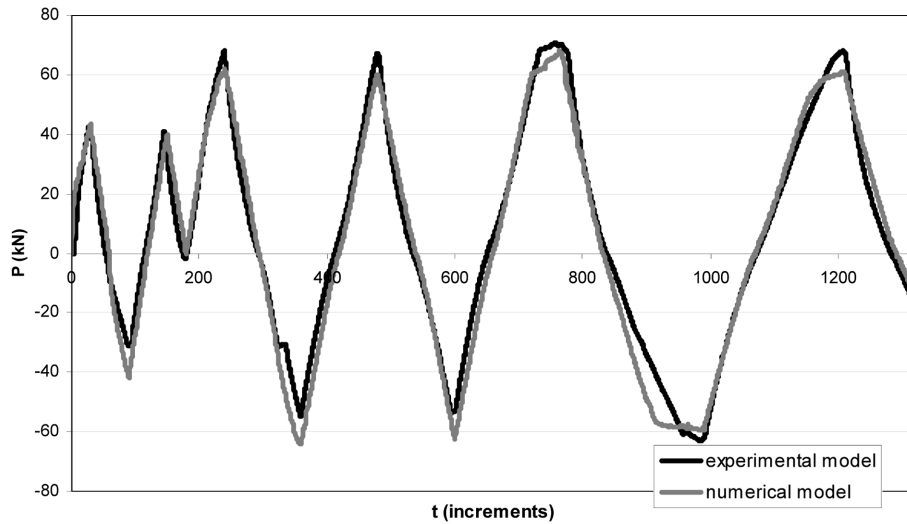


Fig. 18 Comparison of the numerical (2D model) and experimental results of the conventional RC beam under static fully reversing cyclic 4-point bending

The 2D model of the original RC beam specimen under static fully reversing cyclic 4-point bending was then simulated and the results were compared to the corresponding experimental ones. The numerical and experimental results are compared in Figs. 17 and 18 for the cases of monotonic and cyclic loading, respectively. The numerical results are very close to the experimental ones and thus, it is verified that the above problem can be effectively simulated by means of the simple 2D model.

## 6. Behaviour of strengthened beams under static monotonic loading

After validating the numerical model for the RC beam, the numerical models of the strengthened beam specimens were created, according to the principles presented in Section 4. Fig. 19 shows the load-displacement curves for the J1 beam specimen obtained by the 2D numerical model together with the experimental results. There is a very good agreement between the two curves, regarding the overall stiffness of the system, the opening of the first crack, the value of the load at the steel's yielding point and the values of the respective displacements. Very early, a vertical jump appears in the diagram (point A), which corresponds to the loss of the tensile strength of the matrix. This is the point where the first cracks appear. Point B corresponds to the yielding of the reinforcement steel. After that point, the overall strength of the system continues to increase due to the contribution of the fibres, until the maximum strength of the system is attained (point C). Then, the steel fibres fail by being pulled-out and this is represented by an abrupt descending branch in the numerically obtained curve in Fig. 19. The experimental curve exhibits also loss of strength, but more gradually and does not have an abrupt vertical branch. After the loss of the contribution of the steel fibres, the load is undertaken by the longitudinal steel reinforcement. Finally, the longitudinal reinforcement reaches its ultimate tensile capacity leading to the collapse of the specimen.

Based on the numerical analysis, the results on cracking development for several displacement values are presented in Fig. 20. For a displacement of 1 mm, the first cracking appears. Then,

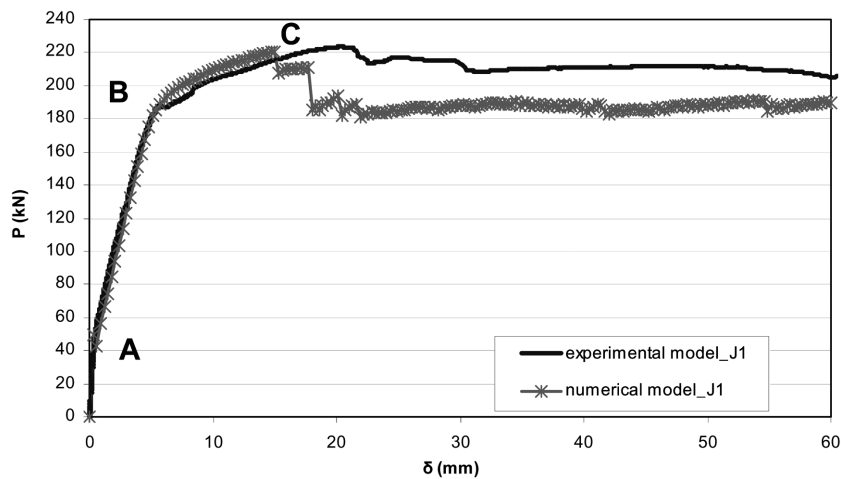


Fig. 19 Comparison of the numerical and experimental results of the conventional RC beam strengthened with the FRCM jacket (J1), under static monotonic 4-point bending

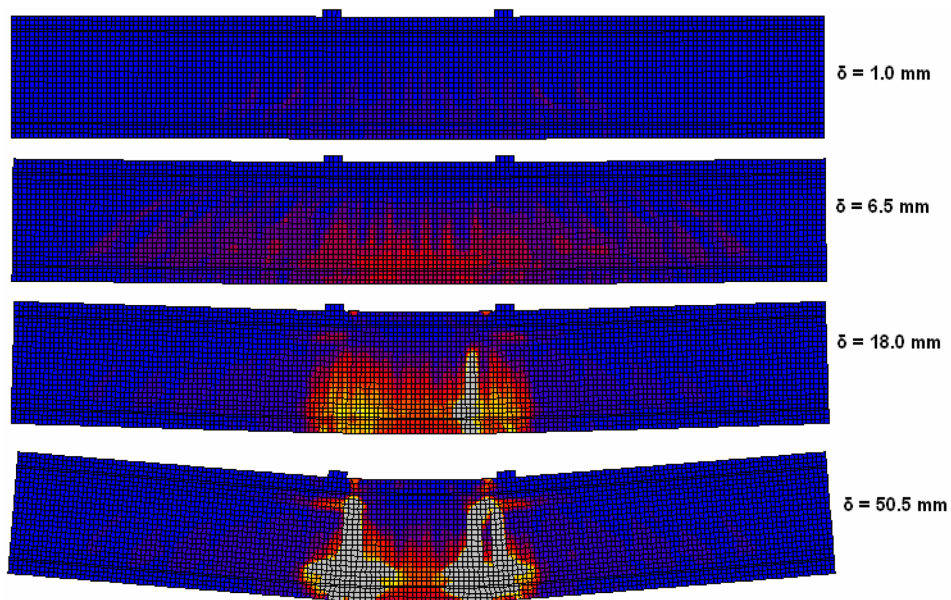


Fig. 20 Cracking strain distribution of the RC beam strengthened with the FRCM jacket (J1), at selected values of mid-span beam deflection  $\delta$

cracking evolves in the cementitious matrix up to a displacement of 6.5 mm at which point yielding begins. The vertical jump that appears in the load-displacement diagram corresponds to the abrupt opening of the main crack and the failure of the steel fibres which occurs for a displacement of 18.0 mm. Finally, the excessive cracking leads actually to the failure of the specimen. Fig. 21 shows the failure of the tested specimen.

The load-displacement curves obtained by the 2D numerical models and the respective tests concerning the J2, J3 and J4 beam specimens are shown in Figs. 22(a), (b) and (c). It can be again noticed that the numerical curves are, in general, in quite good agreement with the experimental ones.



Fig. 21 Failure of the RC beam strengthened with the FRCM jacket (J1), under static monotonic 4-point bending

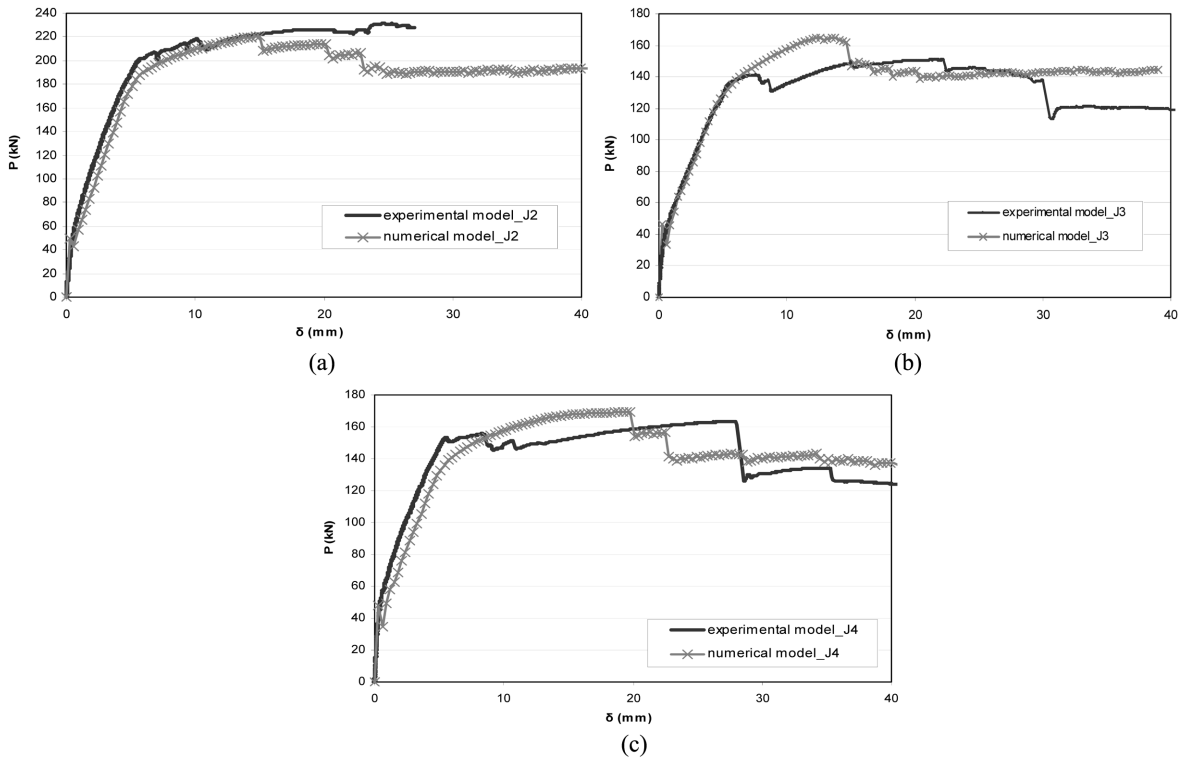


Fig. 22 Comparison of the numerical and experimental results of the RC beam strengthened by the FRCM jacket (a) J2, (b) J3 and (c) J4, under static monotonic 4-point bending

Fig. 23 gives the results obtained by all four numerical analyses (in terms of moment-displacement curves) with respect to those of the original RC specimen. As expected, the strengthening of the RC specimen with the under study jackets results in a significant increase of the strength and stiffness of the original RC specimen, maintaining at the same time the member's deformation capacity. It is worth noting that the strengthened member sustained in the experiments a

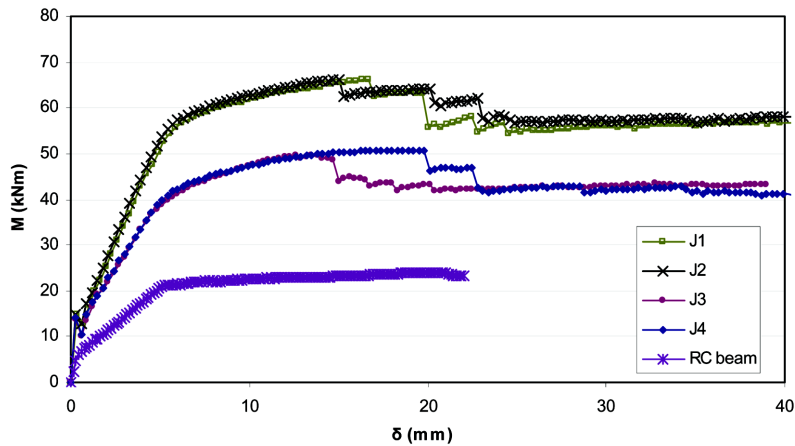


Fig. 23 Applied moment vs. displacement curves predicted by the numerical models for all beam specimens

midspan displacement of more than 60 mm. In some cases the numerical analysis could not follow such displacement ranges due to the excessive cracking that occurred.

In terms of strength, the bending capacity of the jacketed member is nearly 2 to 3 times greater than that of the original RC one. Notice also that, as far as the type of the jacket's reinforcement is concerned, the ultimate load capacity of the members strengthened with the jackets reinforced with the light mesh is significantly lower than that when longitudinal and transverse reinforcement is used. However, the experimental and numerical results confirm that a significant increase of strength can be obtained even with the use of light structural mesh. In any case, the overall behaviour seems not to be affected by the lack of shear reinforcement in the core member.

## 7. Behaviour of strengthened beams under cyclic loading

The next step was to simulate the strengthened specimens under fully reversing cyclic 4-point bending. Figs. 24(a), (b), (c) and (d) show the comparison between the load vs. time curves obtained by the 2D numerical model for the J1, J2, J3 and J4 beam specimens and the corresponding experimental results and it can be concluded that there is a good agreement between them. In terms of ultimate load capacity, the values predicted by the numerical model are in good agreement with the experimental results.

The load-displacement curves obtained from the numerical analysis and from the experiments of the first two cases (J1, J2) are shown in Fig. 25. In the same figure, the results obtained for the case of the RC beam are also presented for comparison reasons. It can be noticed that the hysteresis response is similar for both cases. It is evident that the ultimate load capacity of the strengthened RC beam is almost tripled with respect to that of the original RC beam and it is not affected by the lack of transverse reinforcement in the form of stirrups in the core member. Similar conclusions are derived from the curves of Fig. 26, where the results obtained from the numerical analysis and the tests of J3 and J4 beam specimens are compared. The flexural capacity of the strengthened beam specimen by an FRCM jacket with a steel wire mesh is more than 2 times that of the original RC beam. It should be noted, however, that in the cases where the steel wire mesh is used as reinforcement in the jacket, the load-carrying capacity of the strengthened beam, as well as the

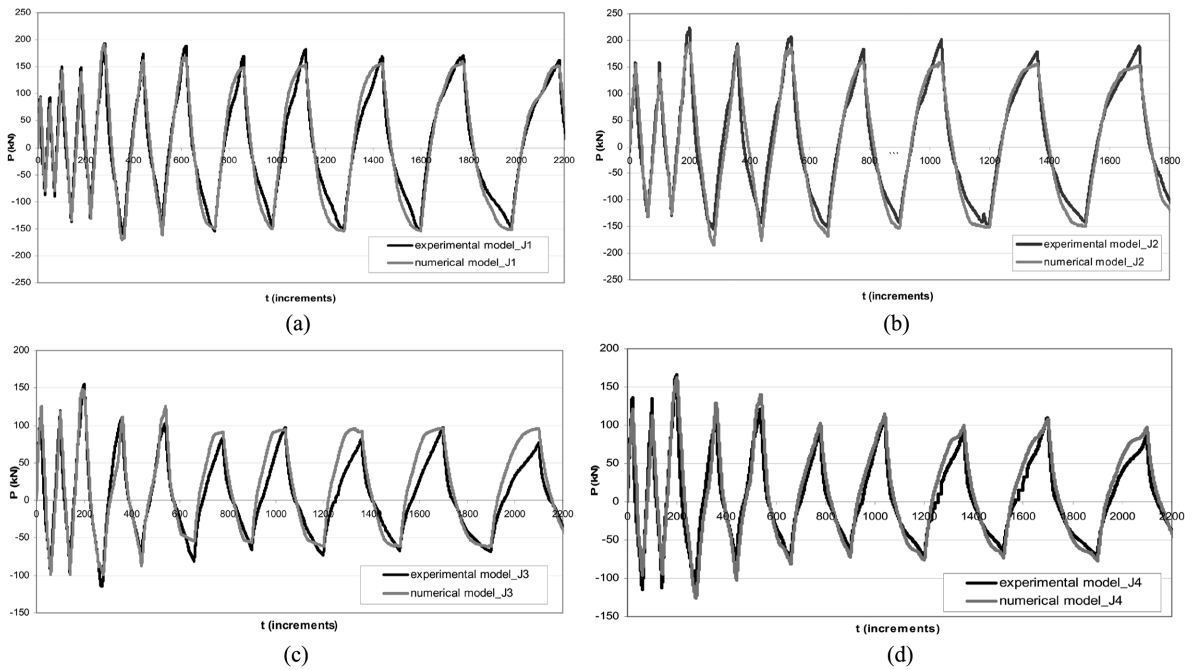


Fig. 24 Comparison of the numerical and experimental results of a RC beam strengthened by the FRCM jacket: (a) J1, (b) J2, (c) J3 and (d) J4, under static fully reversing cyclic 4-point bending

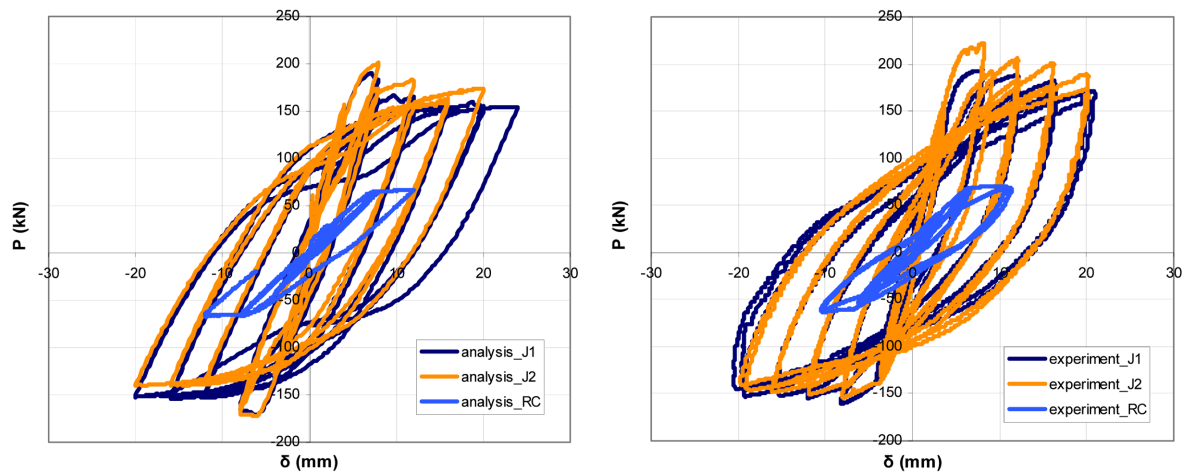


Fig. 25 Numerical and experimental load-displacement curves of the original RC beam and the strengthened RC beams with the FRCM jackets (J1 and J2)

hysteresis loops are rather sensitive to the specific layout of the wire mesh. It should be also mentioned that the absence of transverse reinforcement in the core RC member for the J2 and J4 beam specimens does not seem to have any influence on the hysteretic response of the strengthened members.

In Fig. 27 the numerical and experimental results of J1 and J3 beam specimens are compared, while the results for the behaviour of J2 and J4 beams under cyclic load are shown in Fig. 28. It

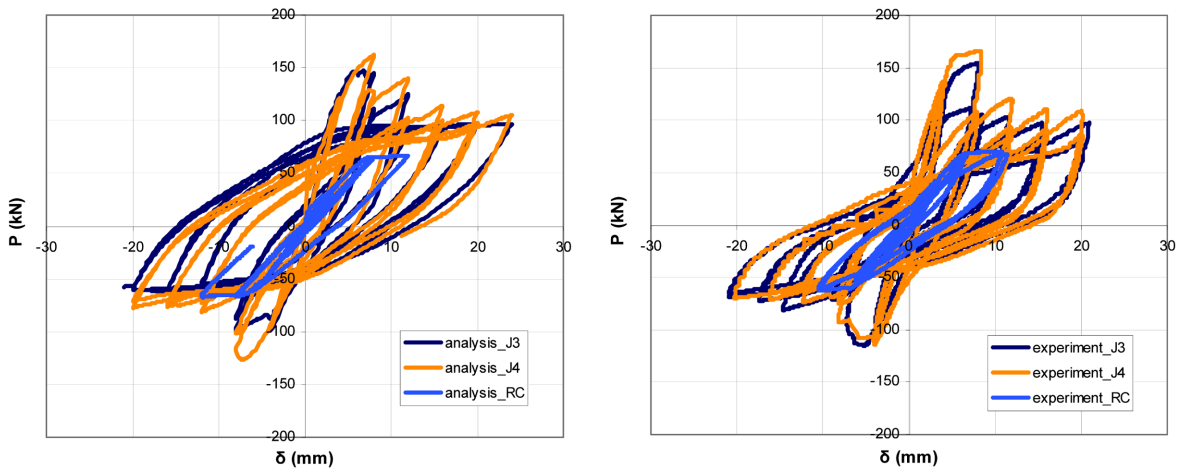


Fig. 26 Numerical and experimental load-displacement curves of the original RC beam and the strengthened RC beams with the FRCM jackets (J3 and J4)

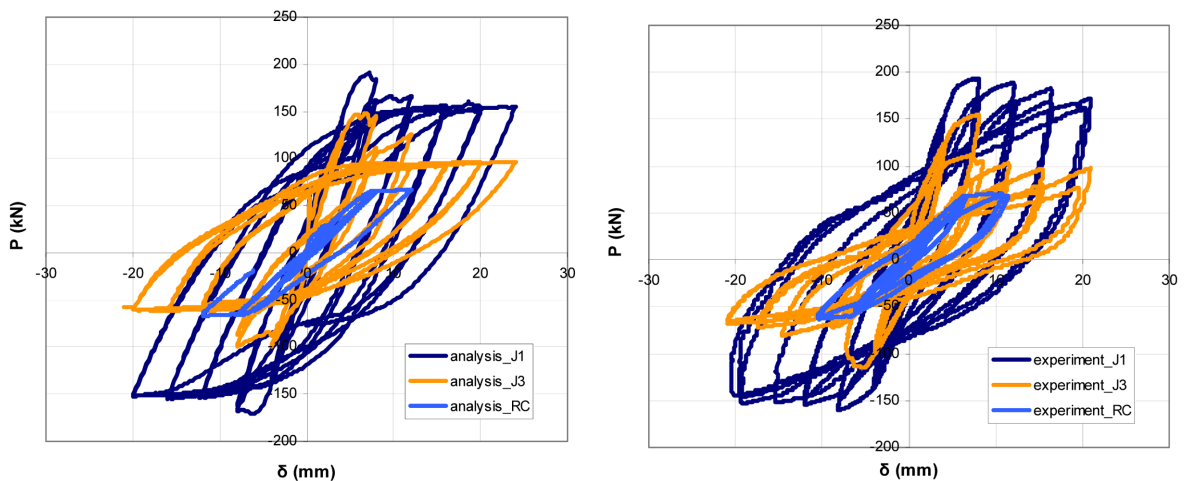


Fig. 27 Numerical and experimental load-displacement curves of the original RC beam and the strengthened RC beams with the FRCM jackets (J1 and J3)

can be observed that after the initial cycles, the load-carrying capacity of the strengthened beams decreases. However, when the FRCM jacket is reinforced with the steel mesh this decrease occurs far more rapidly. From the figures, the superior behaviour of the jackets reinforced with longitudinal and transverse reinforcement (J1 and J2 beam specimens) with respect to the one of the specimens reinforced with the wire mesh (J3 and J4), is also evident. Moreover, the hysteresis loops obtained by the analysis and the experiments of J3 and J4 specimens appear to be less stable with respect to those obtained by the analysis and the tests of the two first cases.

Finally, we have to notice that the approach selected to model cracking (smeared cracking) is well known that may lead to strain localization problems (Bažant and Planas 1998). However, the crack patterns obtained numerically, as well as the overall response of the considered specimens, both in the cases of monotonic and cyclic loading, fit rather well with the corresponding experimental

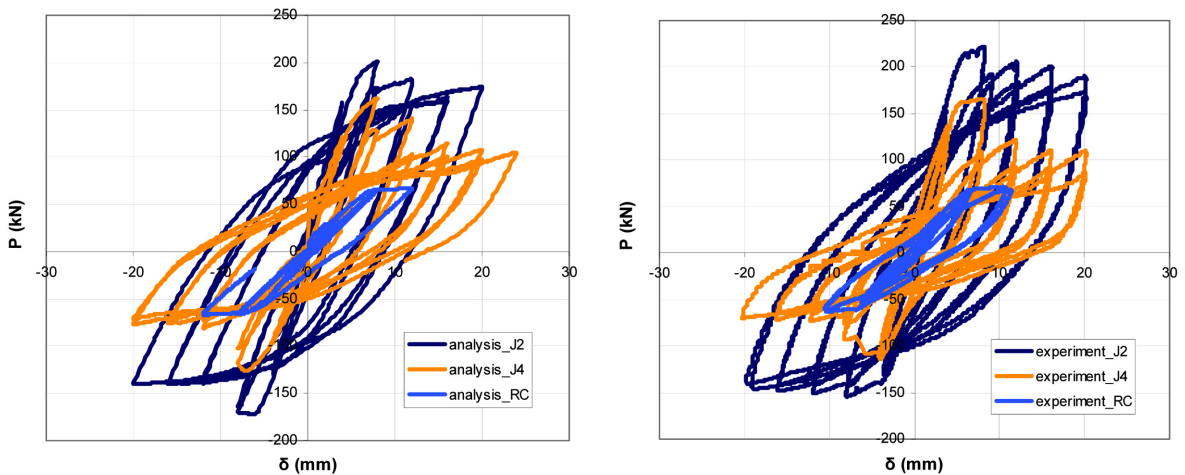


Fig. 28 Numerical and experimental load-displacement curves of the original RC beam and the strengthened RC beams with the FRCM jackets (J2 and J4)

results. Therefore, strain localization problems seem not to affect strongly the results in the specific cases examined here.

## 8. Conclusions

This is a study focusing on the numerical simulation of the behaviour of RC beam specimens with longitudinal steel reinforcement and closely spaced stirrups or no stirrups, strengthened with thin cementitious fibre matrix jackets, reinforced with conventional steel reinforcement or steel wire mesh. Four different types of specimens were tested under static monotonic and fully reversing cyclic 4-point bending. The respective finite element simulation models were formulated and the numerical results were then compared to the experimental ones. It can be concluded that for every case treated here, the numerically obtained load-displacement curves model the experimental results in a very satisfactory way. Also, the crack formation patterns yielded by the finite element analysis show a similar behavior as the experimental results. Therefore, it is concluded that the proposed finite element models can simulate rather accurately the failure mechanism of conventional RC beam specimens strengthened by thin FRCM jackets and can predict an ultimate load capacity very close to that measured in the experiments.

Furthermore, it is evident that, as expected, there is a high increase in the overall strength and stiffness of a conventional RC beam member after strengthening it with a thin FRCM jacket. The results obtained by both the experimental and numerical investigations verify that when longitudinal and transverse reinforcement is used in the jacket instead of wire mesh, a significantly higher load-carrying capacity is achieved. Especially, in the case of cyclic 4-point bending, the hysteresis loops obtained by members strengthened with FRCM jackets with light mesh present lower quality, are less stable and pinching occurs after the first few cycles, indicating a worse hysteretic behaviour.

Another observation is that the lack of shear reinforcement in the core RC beam specimen does not affect the load-carrying capacity and the overall behaviour of the strengthened beam specimens in any way. This is important since the main application of the examined FRCM jackets is the

strengthening of members of existing buildings, which may be designed according to older regulations and thus, having inadequate shear reinforcement. In any case, the application of FRCM jackets should be used guided by an appropriate performance-based design procedure to identify the deficiencies in the existing structure and verify the suitability of the overall strengthening strategy.

## References

- Adhikary, B.B. and Mutsuyoshi, H. (2006), "Shear strengthening of RC beams with web-bonded continuous steel plates", *Constr. Build. Mater.*, **20**(5), 296-307.
- Ashour, S.A. and Wafa, F.F. (1993), "Flexural behavior of high-strength fiber reinforced concrete beams", *ACI Struct. J.*, **90**(3), 279-287.
- Balaguru, P., Narahari, R. and Patel, M. (1992), "Flexural toughness of steel fiber reinforced concrete", *ACI Mater. J.*, **89**(6), 541-546.
- Banthia, N. and Trottier, J.F. (1995), "Concrete reinforced with deformed steel fibers Part II: Toughness Characterization", *ACI Mater. J.*, **92**(2), 146-154.
- Bažant, Z. and Planas, J. (1998) *Fracture and size effects in concrete and other quasibrittle materials*, CRC Press, Florida.
- Bentur, A. and Mindess, S. (1983), "Concrete beams reinforced with conventional steel bars and steel fibres: properties in static loading", *Int. J. Cement Compos. Lightweight Concrete*, **5**(3), 199-202.
- Chunxiang, Q. and Patnaikuni, I. (1999), "Properties of high-strength steel fiber-reinforced concrete beams in bending", *Cement Concrete Comp.*, **21**(1), 73-81.
- Daniel, L. and Loukili, A. (2002), "Behavior of high-strength fiber-reinforced concrete beams under cyclic loading", *ACI Struct. J.*, **99**(3), 248-256.
- deBorst, R., Remmers, J., Needleman, A. and Abellan, M.A. (2004), "Discrete vs smeared crack models for concrete fracture: bridging the gap", *Int. J. Numer. Anal. Method. Geomech.*, **28**(7-8), 583-607.
- Dogan, E. and Krstulovic-Opara, N. (2003), "Seismic retrofit with continuous slurry-infiltrated mat concrete jackets", *ACI Struct. J.*, **100**(6), 713-722.
- Doran, B., Koksai, H. O. and Turgay, T. (2009), "Nonlinear finite element modelling of rectangular/square concrete columns confined with FRP", *Mater. Design*, **30**(8), 3066-3075.
- Georgiadi-Stefanidi, K., Mistakidis, E., Pantousa, D. and Zygomalas, M. (2010), "Numerical modelling of the pull-out of hooked steel fibres from high-strength cementitious matrix, supplemented by experimental results", *Constr. Build. Mater.* (accepted)
- Haddad, R.H., Shannag, M.J. and Hamad, R.J. (2007), "Repair of heat-damaged reinforced concrete T-beams using FRCM jackets", *Mag. Concrete Res.*, **59**(3), 223-231.
- Khalifa, A. and Nanni, A. (2002), "Rehabilitation of rectangular simply supported RC beams with shear deficiencies using CFRP composites", *Constr. Build. Mater.*, **16**(3), 135-146.
- Krstulovic-Opara, N. and Al-Shannag, M.J. (1999), "Slurry infiltrated mat concrete (SIMCON)-based shear retrofit of reinforced concrete members", *ACI Struct. J.*, **96**(1), 105-114.
- Li, J., Gong, J. and Wang, L. (2009), "Seismic behaviour of corrosion-damaged reinforced concrete columns strengthened using combined carbon fiber-reinforced polymer and steel jacket", *Constr. Build. Mater.*, **23**(7), 2653-2663.
- Li, V.C. (2003), "On engineered cementitious composites (ECC). A review of the material and its applications", *J. Adv. Concrete Technol.*, **1**(3), 215-230.
- Naaman, A.E. and Reinhardt, H.W. (1996), "Characterization of high performance fiber reinforced cement composites-HPFRCCM", In: Naaman AE, Reinhardt HW, editors. *High Performance Fiber Reinforced Cement Composites 2 (HPFRCCM 2), Proceedings of the Second International RILEM Workshop*, E&FN Spon, London, 1-24.
- Naaman, A.E., Reinhardt, H.W. and Fritz, C. (1993), "Reinforced concrete beams with SIFCON matrix", *ACI Struct. J.*, **89**(1), 1-15.
- Oluokun, A.F. and Haghayeghi, A.R. (1998), "Flexural behavior of reinforced concrete beams retrofitted or

- repaired with slurry infiltrated mat concrete”, *ACI Struct. J.*, **95**(6), 654-664.
- Padmarajaiah, S.K. and Ramaswamy, A. (2002), “A finite element assessment of flexural strength of prestressed concrete beams with fibre reinforcement”, *Cement Concrete Comp.*, **24**(2), 229-241.
- Papanikolaou, V.K. and Kappos, A.J. (2007), “Confinement-sensitive plasticity constitutive model for concrete in triaxial compression”, *Int. J. Solids Struct.*, **44**(21), 7021-7048.
- Papatheocharis, T.T. and Perdikaris, P.C. (2009), “Experimental study of the behavior of conventional RC beams reinforced with fiber-reinforced-cement jackets”, *16<sup>th</sup> National Greek Conference of Concrete Structures*, Pafos, Cyprus, October. (in Greek)
- Paramasivam, P., Lim, C.T. and Ong, K.C. (1998), “Strengthening of RC beams with ferrocement laminates”, *Cement Concrete Comp.*, **20**(1), 53-65.
- Rodriguez, M. and Park, R. (1994), “Seismic load tests on reinforced concrete columns strengthened by jacketing”, *ACI Struct. J.*, **91**(2), 150-159.
- Shannag, M.J. and Alhassan, M.A. (2005), “Seismic upgrade of interior beam-column subassemblages with high-performance fiber-reinforced concrete jackets”, *ACI Struct. J.*, **102**(1), 131-138.
- Triantafyllou, T.C. and Papanicolaou, C.G. (2006), “Shear strengthening of reinforced concrete members with textile reinforced mortar (TRM) jackets”, *Mater. Struct.*, **39**(1), 93-103.
- Vandoros, K.G. and Dritsos, S.E. (2006), “Concrete jacket construction detail effectiveness when strengthening RC columns”, *Constr. Build. Mater.*, **22**(3), 264-276.